Complex networks with complex weights

Lucas Böttcher[1, *] and Mason A. Porter[2, 3, †]

[1] *Centre for Human and Machine Intelligence, Frankfurt School of Finance and Management, 60322 Frankfurt am Main, Germany*
[2] *Department of Mathematics, University of California, Los Angeles, CA, 90095, United States of America*
[3] *Santa Fe Institute, Santa Fe, NM, 87501, United States of America*

(Dated: December 14, 2022)

In many scientific applications, it is common to use binary (*i.e.*, unweighted) edges in the study of networks to examine collections of entities that are either adjacent or not adjacent. Researchers have generalized such binary networks to incorporate edge weights, which allow one to encode node–node interactions with heterogeneous intensities or frequencies (*e.g.*, in transportation networks, supply chains, and social networks). Most such studies have considered real-valued weights, despite the fact that networks with complex weights arise in fields as diverse as quantum information, quantum chemistry, electrodynamics, rheology, and machine learning. Many of the standard approaches from network science that originated in the study of classical systems and are based on real-valued edge weights cannot be applied directly to networks with complex edge weights. In this paper, we examine how standard network-analysis methods fail to capture structural features of networks with complex weights. We then generalize several network measures to the complex domain and show that random-walk centralities provide a useful tool to examine node importances in networks with complex weights.

I. INTRODUCTION

Network representations of complex systems can provide useful insights into the structural organization of numerous physical, biological, and social phenomena [1]. For more than two decades, research in network science has focused on the development of methods to analyze structural features of networks and their effects on dynamical processes (including opinions and social influence, the spread of infectious diseases, and synchronization [2]) on networks. If information on the intensity of interactions (and hence on the coupling strength) between nodes is unavailable, unweighted networks provide a reasonable starting point to analyze structural features of systems (such as peer-to-peer networks and social networks) in which one can describe nodes as either either in contact (or otherwise interacting) or not in contact. However, in many applications, it is useful to use edge weights to account for the intensity or frequency of interactions between pairs of nodes. For example, researchers have used weighted edges to describe the contact frequencies between individuals in human contact networks [3] and passenger flows in air-transportation networks [4]. In the study of signaling pathways in proteins, weighted networks can help model interactions between different parts of a molecule [5].

The vast majority of research on weighted networks has focused on networks with real-valued edge weights [4, 6–9] and node weights [10]. However, networks with complex weights arise in a variety of scientific and engineering applications (see Tab. I), and it is necessary to adapt and reformulate existing network-analysis methods to analyze them. Complex numbers arise in classical physics (*e.g.*, in fluid dynamics and in electrodynamics) to simplify mathematical descriptions of wave-like phenomena. In quantum physics [11–13], one defines wave functions and their unitary evolution in complex vector spaces. Moreover, recent experiments provide strong evidence that real-valued formulations of the standard framework of quantum physics [14] fail to capture physical reality [15–17].

In quantum physics, one can think of Hermitian matrices that are associated with the Hamiltonian of an isolated quantum system as an adjacency matrix with real-valued diagonal terms (*i.e.*, energy terms) and complex-valued off-diagonal terms, which describe changes in amplitude during a transition from one state to another. The connection between modularity maximization and node-occupation properties of random walks has been used to identify communities in such networks [18]. In addition to applying network-analysis methods to isolated quantum systems, it is also possible to study quantum networks that one can construct using entangled states and physically interconnected subsystems [19].

In electrodynamics, one can interpret a network with real-valued edge weights as a network of resistors with weights that represent resistance values. One can use complex weights to describe impedance and admittance values in more general networks, such as in lumped-element models of coupled transmission lines [20, 21], that include resistors, coils, and capacitors.

The use of complex weights can substantially improve the performance of artificial neural networks in comparison to their real-valued counterparts with respect to accuracy, convergence, and their ability to produce nonlinear decision boundaries (even for small numbers of

* l.boettcher@fs.de
† mason@math.ucla.edu

Subject	Applications	$W = W^\dagger$	References
Quantum information	Description of quantum walks	✓	[22–26]
Condensed-matter physics	Electron transport in quantum networks; interactions between electrons and magnetic fields	✗✓	[27–30]
Mathematical chemistry	Structural properties of molecules	✗✓	[31–33]
Electrodynamics	Impedance values and reflection/transmission coefficients in transmission-line networks	✗	[20, 21, 34]
Electrostatics	Complex permittivities and permeabilities*	✗	[34]
Rheology	Complex storage and loss moduli of viscoelastic materials*	✗	[35]
Computational social science	Social-network analysis	✓	[36]
Machine learning	Complex-valued optical neural networks; graph neural networks; graph signal processing	✗✓	[37–41]
Linear algebra	Study of Hermitian directed graphs	✓	[42–45]

TABLE I. **Summary of a variety of application areas of networks with complex weights.** For the described applications in electrostatics and rheology (which we mark with *), one can use complex node weights to describe heterogeneous materials that are subject to heterogeneous electromagnetic and force fields. All other listed applications primarily use edge weights. A ✓ indicates that a subject includes examples with Hermitian weight matrices, and a ✗ indicates that a subject includes examples with non-Hermitian weight matrices.

neurons) [37].[1]

In Tab. I, we indicate several application areas of networks with complex edge weights and/or complex node weights. This table is not a rigid classification; instead, it summarizes a variety of areas in which complex adjacency matrices arise. Because of the connection between complex adjacency matrices and network descriptions of quantum transport of charged particles [29, 46], researchers also use the term "magnetic adjacency matrix" in this context [47, 48]. One can use magnetic adjacency matrices to construct "magnetic Laplacians", which have been integrated into spectral graph neural networks to study node-classification and edge-prediction tasks in directed networks [38, 39]. Many of the related works that we list in Tab. I focus on Hermitian weight matrices W (which satisfy $W = W^\dagger$). Complex weight matrices in electrodynamics, electrostatics, and materials science may not be Hermitian, as they describe heterogeneous materials or materials that are subject to heterogeneous fields.

In the present paper, we examine several issues with the application of standard network-analysis methods to networks with complex weights. We also examine a variety of connections to related physical systems that help us interpret the meaning of complex weight matrices (*i.e.*, weighted adjacency matrices). In Sec. II, we give a mathematical definition of networks with complex weights and we then discuss the relationship between such networks and random walks and information consensus [49]. As analogs of classical random walks and DeGroot consensus dynamics, we show that Hermitian complex weight matrices induce continuous-time quantum walks (CTQWs) and phase-synchronization dynamics that are related to the Schrödinger–Lohe model, which is a generalization of Kuramoto dynamics to non-Abelian oscillators and quantum oscillators [50–54]. In Sec. III, we identify another connection to phase synchronization by defining appropriate local network measures [4], such as a complex-valued node strength and a complex-valued weighted clustering coefficient.

In Sec. IV, we extend our discussion of walks in networks with complex weights and explain that one can interpret walks and their associated complex weights in terms of (1) interactions between charged particles and a magnetic field [29] and (2) exchange statistics of indistinguishable particles [55–59]. To mathematically characterize structural differences between networks with binary, real, and complex weights, we study how different weight matrices affect graph energy (*i.e.*, the sum of the absolute values of the eigenvalues of W) in Sec. V. Graph energy is a commonly employed network measure in mathematical chemistry because of its connection to π-electron energy in tight-binding models [60].

One cannot directly apply certain network notions (such

[1] For example, one can use a single layer with two complex-valued neurons to represent conic sections (*i.e.*, parabolas, circles, ellipses, and hyperbolas); a corresponding real-valued layer can only represent linear functions [37].

as eigenvector centrality and its generalizations) to networks with complex edge weights, as one must first have some matrix — a weight matrix or some other matrix, such as a function of the weight matrix — that satisfies the Perron–Frobenius theorem [61, 62], for which we seek a real-valued and positive matrix to ensure that its leading eigenvector has strictly positive entries. In Sec. VI, we discuss a generalization of the Perron–Frobenius theorem [63, 64] and eigenvector centrality. Another constraint that relates to centrality measures arises from the inability to fully order complex numbers. This issue becomes apparent when we think of, *e.g.*, geodesic centrality measures, which are based on shortest paths. Approaches to compute such measures with Dijkstra's algorithm (when edge weights are positive) or the Bellman–Ford algorithm (when edge weights are either positive and negative) rely on comparing ordered quantities [65, 66]. In Sec. VII, we show how to avoid issues that are associated with geodesic centralities by using random-walk centrality measures that allow both real-valued and complex-valued edge weights [24, 67]. Finally, in Sec. VIII, we discuss our results and indicate possible future directions in the study of networks with complex weights.

II. COMPLEX WEIGHTS AND THEIR CONNECTION TO RANDOM WALKS AND INFORMATION CONSENSUS

We consider networks in the form of weighted graphs $G = (V, E, w)$, where V is a set of nodes, E is a set of edges, and the function $w\colon E \to \mathbb{C}$ assigns a complex weight to each edge. The number of nodes is $N = |V|$. In accordance with Ref. [4], we use both an adjacency matrix $A \in \mathbb{R}^{N\times N}$ and a weight matrix (*i.e.*, a weighted adjacency matrix) $W \in \mathbb{C}^{N\times N}$ to describe weighted edges between nodes. The entries a_{ij} of the matrix A are equal to 1 if nodes i and j are adjacent and are equal to 0 if they are not adjacent. Unless we state otherwise, we do not consider self-edges or self-weights. (That is, we take $a_{ii} = w_{ii} = 0$.) To capture complex-valued relations between nodes, we let the weight-matrix entries $w_{ij} = r_{ij}e^{\mathrm{i}\varphi_{ij}}$ be complex numbers with magnitude r_{ij} and phase φ_{ij}. If a network is undirected, then $r_{ij} = r_{ji}$ and $\varphi_{ij} = \varphi_{ji}$. If $a_{ij} = 0$, then we set $w_{ij} = 0$.

In Fig. 1, we show examples of networks with real and complex weights. Both of the depicted networks are closed and directed triads. For a connected network with non-negative real weights w_{ij} [see Fig. 1(a)], we can rescale w_{ij} by mapping $w_{ij} \to w_{ij}/(\sum_{j=1}^{N} a_{ij}w_{ij})$ to obtain a stochastic weight matrix that induces a random walk

$$\frac{\mathrm{d}\mathbf{x}(t)}{\mathrm{d}t} = (W - \mathbb{1})\,\mathbf{x}(t) = -H_{\mathrm{c}}\mathbf{x}(t)\,, \tag{1}$$

where $H_{\mathrm{c}} = \mathbb{1} - W$ is the classical random-walk Hamiltonian and $\mathbf{x}(t)$ is a probability vector with entries $x_j(t)$ (with $j \in \{1, \ldots, N\}$), which give the probabilities of finding a random walker at each node j at time t. Under the aforementioned weight rescaling, one can thus always interpret a connected network with non-negative real weights in terms of transition probabilities of a classical random walker. For the left stochastic weight matrix $W = AD^{-1}$, we obtain $H_{\mathrm{c}} = LD^{-1}$, where $L = D - A$ is the combinatorial graph Laplacian, $D = \mathrm{diag}(k_1, \ldots, k_N)$ is the degree matrix, and $k_i = \sum_j a_{ij}$ is the degree of node i (*i.e.*, the number of neighbors of node i). The stationary state of Eq. (1) for $H_{\mathrm{c}} = LD^{-1}$ yields an occupation centrality measure that is proportional to node degree [24, 68].

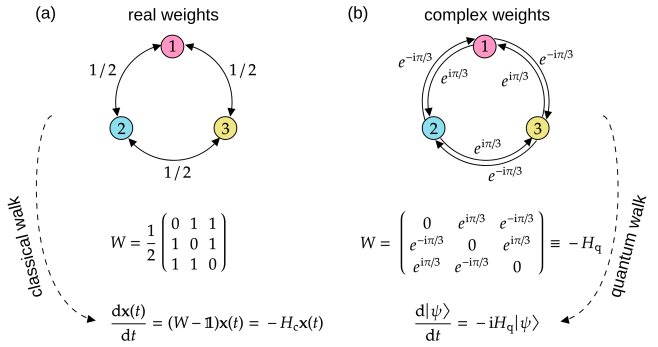

FIG. 1. **Examples of networks with real and complex edge weights**. Each of these networks is a closed and directed triad. (a) The weight matrix W is stochastic. It induces random-walk dynamics $\dot{\mathbf{x}}(t) = -H_{\mathrm{c}}\mathbf{x}(t)$, where $H_{\mathrm{c}} = \mathbb{1} - W$ and $\mathbf{x}(t)$ is a probability vector whose entries $x_j(t)$ (with $j \in \{1, 2, 3\}$) give the probabilities of finding a random walker at each node j at time t. (b) The weight matrix W is Hermitian. It induces a continuous-time quantum walk $|\dot{\psi}\rangle = -\mathrm{i}H_{\mathrm{q}}\,|\psi\rangle$, where $|\psi\rangle \in \mathbb{C}^3$ and $H_{\mathrm{q}} = -W$.

The random-walk evolution (1) is equivalent to the continuous-time DeGroot opinion-consensus model

$$\frac{\mathrm{d}x_i(t)}{\mathrm{d}t} = \sum_{j=1}^{N} a_{ij}\,(x_j(t) - x_i(t)) \tag{2}$$

if we replace $H_{\mathrm{c}} = LD^{-1}$ with $H_{\mathrm{c}} = L$ [69]. In the DeGroot model, we treat the underlying network as undirected (*i.e.*, $a_{ij} = a_{ji}$) and entry $x_i(t)$ indicates the opinion of node i. For a right stochastic weight matrix, such as $W = D^{-1}A$, we obtain

$$\frac{\mathrm{d}x_i(t)}{\mathrm{d}t} = \sum_{j=1}^{N} w_{ij}\,(x_j(t) - x_i(t)) \tag{3}$$

as a generalization of Eq. (2). As in the original continuous-time DeGroot model (2), the nontrivial stationary state $\mathbf{x}^*$ of the weighted model (3) is a consensus state with $x_i^* = x_j^* \equiv x^*$. Unlike in Eq. (2), the quantity $\sum_i x_i(t)$ is, in general, not conserved in Eq. (3) because a stochastic weight matrix is symmetric only for regular graphs (*i.e.*, for graphs in which each node has the same degree).

One can establish a similar connection between weighted networks and linear diffusion dynamics for a network with complex weights [70]. A Hermitian weight matrix W (*i.e.*, a weight matrix that satisfies $W = W^\dagger$) induces a CTQW that satisfies

$$\mathrm{i}\frac{\mathrm{d}\,|\psi\rangle}{\mathrm{d}t} = H_\mathrm{q}\,|\psi\rangle\ , \tag{4}$$

where $|\psi\rangle \in \mathbb{C}^N$ and $H_\mathrm{q} = -W$ [see Fig. 1(b)].

The infinite-time mean

$$\pi_j = \lim_{T\to\infty}\frac{1}{T}\int_0^T \langle j|\rho(t)|j\rangle\ \mathrm{d}t \tag{5}$$

of a CTQW gives an occupation centrality measure for a network with complex edge weights [68]. In Eq. (5), $\mathrm{d}t$ is an infinitesimal time step, $\rho(t) = |\psi(t)\rangle\,\langle\psi(t)|$ is a density operator, and $|j\rangle \in \mathbb{C}^N$ is an orthonormal basis vector that satisfies

$$\langle i|j\rangle = \delta_{ij}\,. \tag{6}$$

We obtain a quantum-mechanical analog of the DeGroot consensus dynamics (2) by setting

$$(H_\mathrm{q})_i = \mathrm{i}\sum_{j=1}^N a_{ij}\left[|\psi_j\rangle\,\langle\psi_i| - |\psi_i\rangle\,\langle\psi_j|\right]\ , \tag{7}$$

which yields

$$\mathrm{i}\frac{\mathrm{d}\,|\psi_i\rangle}{\mathrm{d}t} = \mathrm{i}\sum_{j=1}^N a_{ij}\left[|\psi_j\rangle - \langle\psi_j|\psi_i\rangle\,|\psi_i\rangle\right]\ . \tag{8}$$

Equation (8) preserves $\|\psi_i\|^2 = \langle\psi_i|\psi_i\rangle$ for each state $|\psi_i\rangle$ (see App. A) and synchronizes the relative phases between states $|\psi_i\rangle$ and $|\psi_j\rangle$ (with $i \neq j$). It is a special case of the Schrödinger–Lohe model [50, 51] with the Hamiltonian (7). Other versions of the Schrödinger–Lohe model [52, 53] include a Laplacian term in the Hamiltonian and additional potential functions. Lohe's generalization of Kuramoto dynamics to non-Abelian oscillators and quantum oscillators [50–54] is also connected to recent work on Kuramoto dynamics on high-dimensional spheres [71].

If the states $|\psi_i\rangle$ satisfy $\|\psi_i\|^2 = 1$, then $|\psi_i\rangle = e^{-\mathrm{i}\theta_i(t)}$. Upon rescaling $a_{ij} \to a_{ij}K/(2N)$, Eq. (8) is equivalent to the Kuramoto model

$$\frac{\mathrm{d}\theta_i(t)}{\mathrm{d}t} = \frac{K}{N}\sum_{j=1}^N a_{ij}\sin\left(\theta_j(t) - \theta_i(t)\right) \tag{9}$$

with a homogeneous coupling constant K and a rotating reference frame in which all oscillators have the same natural frequency [72]. The continuous-time DeGroot model (2) corresponds to the linearization of Eq. (9) for small phase differences and $K = N$.

In a network with a complex weight matrix W, we redefine the Hamiltonian (7) as

$$(H_\mathrm{q})_i = \mathrm{i}\sum_{j=1}^N\left[w_{ji}\,|\psi_j\rangle\,\langle\psi_i| - w_{ij}\,|\psi_i\rangle\,\langle\psi_j|\right]\ . \tag{10}$$

The Hamiltonian $(H_\mathrm{q})_i$ in Eq. (10) is Hermitian if and only if W is Hermitian (*i.e.*, when $w_{ij} = \bar{w}_{ji}$ for all i and j). Setting $w_{ji} = Ke^{-\mathrm{i}\alpha}/(2N)$ yields the Sakaguchi–Kuramoto (SK) model[2]

$$\frac{\mathrm{d}\theta_i(t)}{\mathrm{d}t} = \frac{K}{N}\sum_{j=1}^N a_{ij}\sin\left(\theta_j(t) - \theta_i(t) + \alpha\right)\ , \tag{11}$$

where α is the phase lag and $|\alpha| \leq \pi/2$ [73]. The empirical motivation of the phase-lag parameter α is that the common frequency of strongly coupled oscillators typically deviates from the mean natural frequency. The SK model is relevant to various applications, such as for describing the synchronization of coupled electrical oscillators [74].

For classical consensus dynamics like (2) or (3), we quantify the amount of consensus by calculating

$$r_\mathrm{c}(t) = 1 - \frac{1}{2\Gamma}\|\mathbf{x} - \mathbf{x}^*\|_1 \equiv 1 - \frac{1}{2\Gamma}\sum_{i=1}^N |x_i(t) - x_i^*|\,, \tag{12}$$

where $\Gamma = Nx^*$ and $\mathbf{x}^* = (x^*, \ldots, x^*)^\top$ is the consensus state that is associated with (2) or (3).

For the unweighted DeGroot model (2) with $\sum_{i=1}^N x_i(0) = 1$, we have $x^* = 1/N$ (with $i \in \{1, \ldots, N\}$) and $\lim_{t\to\infty} r_\mathrm{c}(t) = 1$. At time $t = 0$, the consensus $r_\mathrm{c}(0)$ reaches a minimum $1/N$ for $x_i(0) = 1$ and $x_j(0) = 0$ (with $j \neq i$). In this minimum, the opinion of one node deviates maximally from the opinions of the other nodes. For the weighted DeGroot model (3), the stationary state is $\mathbf{x}^* = \lim_{t\to\infty} e^{(W-\mathbb{1})t}\mathbf{x}(0)$.

For $|\psi_i\rangle = e^{-\mathrm{i}\theta_i(t)}$, the corresponding order parameter of the quantum consensus dynamics (8) is

$$\begin{aligned} r_\mathrm{q}(t)^2 &= 1 - \frac{1}{2N^2}\sum_{i,j}\|\psi_i - \psi_j\|^2 = \frac{1}{N^2}\sum_{i,j} e^{\mathrm{i}(\theta_j(t) - \theta_i(t))} \\ &= \frac{1}{N^2}\sum_{i,j}\cos\left(\theta_j(t) - \theta_i(t)\right)\ , \end{aligned} \tag{13}$$

where $r_\mathrm{q}(t)$ is equivalent to the order parameter of the Kuramoto model [72].

In Figure 2, we show the evolution of $r_\mathrm{c}(t)$ and $r_\mathrm{q}(t)$ for classical and quantum consensus dynamics on a $G(N, p)$ Erdős–Rényi (ER) network with $N = 100$ nodes and connection probability $p = 0.2$ (for an edge to exist between two nodes). The solid black and dashed orange curves give the dynamics for unweighted and weighted consensus, respectively. For the weighted DeGroot model (3), we set $w_{ij} = a_{ij}/k_i$. Additionally, we set $w_{ji} = e^{\mathrm{i}\pi/4}$ and

[2] We use the term "Sakaguchi–Kuramoto model" because Ref. [73] lists Sakaguchi and Kuramoto as first and second authors, respectively. Some papers use the term "Kuramoto–Sakaguchi model" to refer to the same model.

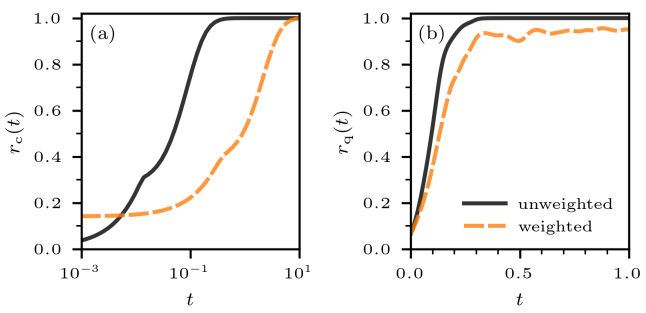

FIG. 2. **Classical and quantum consensus.** The evolution of the (a) classical consensus (12) and (b) quantum consensus (13). The underlying network is a $G(N,p)$ Erdős–R??nyi (ER) network with $N = 100$ nodes and connection probability $p = 0.2$. The solid black and dashed orange curves indicate the unweighted and weighted consensus dynamics, respectively. For the weighted DeGroot model (3), we set $w_{ij} = a_{ij}/k_i$. Additionally, we set $w_{ji} = e^{\mathrm{i}\pi/4}$ and $w_{ij} = e^{-\mathrm{i}\pi/4}$ in the weighted Hamiltonian (10). In panel (a), we compute $\mathbf{x}(t)$ in $r_c(t)$ by evaluating $e^{(W-\mathbb{1})t}\mathbf{x}(0)$, where $x_1(0) = 1$ and $x_j(0) = 0$ for $j \in \{2,\ldots,N\}$. In panel (b), we use an implicit unitary integrator to solve Eq. (4) with Hamiltonian (10). We normalize each initial wave-function component $|\psi_i(0)\rangle$ (with $i \in \{1,\ldots,N\}$) to 1, and we uniformly-randomly distribute their phases with mean $\pi/3$ and variance $25/3$.

$w_{ij} = e^{-\mathrm{i}\pi/4}$ in the weighted Hamiltonian (10). The unweighted consensus dynamics in Fig. 2 reach values $r_c(t)$ and $r_q(t)$ near 1 faster than their weighted counterparts. We also observe that the complex weights $e^{\pm\mathrm{i}\pi/4}$ in the Hamiltonian (10) are associated with smaller consensus values than in the unweighted consensus dynamics.

III. LOCAL NETWORK MEASURES

Because the entries w_{ij} of W are complex-valued, the strength

$$s_i = \sum_{j=1}^{N} w_{ij} \tag{14}$$

of node i is also a complex quantity. In contrast to real-valued edge weights [4], s_i does not provide a measure of importance or centrality of node i because one cannot fully order complex numbers.

To quantify the distribution of complex weights of the edges that are attached to node i, we define the normalized strength of node i as

$$\bar{s}_i = \frac{s_i}{k_i} = \frac{\sum_{j=1}^{N} w_{ij}}{\sum_{j=1}^{N} a_{ij}} . \tag{15}$$

How do different values of the amplitudes r_{ij} and phases φ_{ij} affect the value of $\bar{s}_i$? To answer this question, we

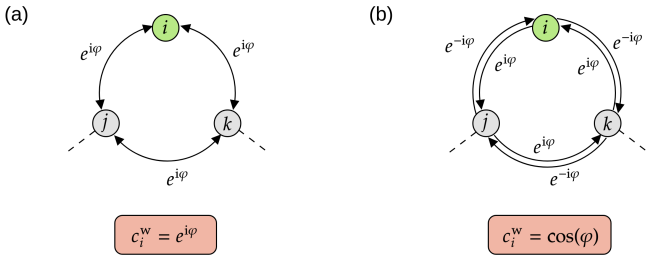

FIG. 3. **Examples of clustering coefficients in a network with complex edge weights.** (a) A closed and directed triad with complex weights $e^{\mathrm{i}\varphi}$. The weighted clustering coefficient of node i (in green) is $c_i^{\mathrm{w}} = e^{\mathrm{i}\varphi}$. (b) A closed and directed triad with complex weights $e^{\pm\mathrm{i}\varphi}$. The weighted clustering coefficient of node i (in green) is $c_i^{\mathrm{w}} = \cos(\varphi)$.

first consider the case in which $r_{ij} = 1$ for all i and j. For $a_{ii} = w_{ii} = 0$ and $r_{ij} = 1$, we have

$$\bar{s}_i = \frac{1}{k_i}\sum_{j=1}^{N} a_{ij} e^{\mathrm{i}\varphi_{ij}} , \tag{16}$$

so

$$|\bar{s}_i|^2 = \frac{1}{k_i^2}\sum_{j,l} e^{\mathrm{i}(\varphi_{ij}-\varphi_{il})} = \frac{1}{k_i^2}\sum_{j,l}\cos(\varphi_{ij}-\varphi_{il}) . \tag{17}$$

Observe that $|\bar{s}_i|^2 = 1$ if $\varphi_{ij} = \varphi_{il}$ for all edges that are attached to node i and that $\bar{s}_i$ reaches a minimum if all phases are balanced around the unit circle (*e.g.*, if they are spread evenly or distributed in clusters that balance each other). For phase distributions other than these two cases, $|\bar{s}_i|^2$ satisfies $0 < |\bar{s}_i|^2 < 1$. When $r_{ij} = 1$, Eq. (17) implies that complex weights induce a local node quantity that is similar to the order parameter of the Kuramoto model [see Eq. (13)].

If $r_{ij} = r$, then $0 < |\bar{s}_i|^2 < r^2$. Additionally, for general distributions of r_{ij} with $r_{\max} = \max_{i,j}(r_{ij})$, we find that $0 < |\bar{s}_i|^2 < r_{\max}^2$.

Directly generalizing the definition of weighted nearest-neighbor degree from Ref. [4] to networks with complex edge weights yields

$$k_{\mathrm{nn},i}^{w} = \frac{1}{s_i}\sum_{j=1}^{N} w_{ij}k_j . \tag{18}$$

One may wish to separately track real and imaginary nearest-neighbor degrees by calculating $\mathrm{Re}(k_{\mathrm{nn},i}^{w})$ and $\mathrm{Im}(k_{\mathrm{nn},i}^{w})$.

In an unweighted and undirected network, the local clustering coefficient [75] of node i is

$$c_i = \frac{1}{k_i(k_i-1)}\sum_{j,k} a_{ij}a_{jk}a_{ki} \tag{19}$$

when $k_i \geq 2$. For $k_i = 0$ and $k_i = 1$, we set $c_i = 0$. There are a variety of ways to define local clustering coefficients

in weighted networks [4, 7, 8]. Drawing inspiration from Ref. [7], we define the local weighted clustering coefficient of a directed network with complex weights as

$$c_i^{\mathrm{w}} = \frac{1}{k_i(k_i-1)} \sum_{j,k} (\tilde{w}_{ij}\tilde{w}_{jk}\tilde{w}_{ki})^{1/3}\,, \tag{20}$$

where $\tilde{w}_{ij}$ denotes the weight between nodes i and j, normalized by the maximum magnitude $\max_{i,j}|w_{ij}| = \max_{i,j}|r_{ij}|$. That is, $\tilde{w}_{ij} = w_{ij}/\max_{i,j}|w_{ij}|$. The weighted clustering coefficient c_i^{w} is a complex number that satisfies $|c_i^{\mathrm{w}}| = 1$. For $w_{ij} = ra_{ij}$ with $r > 0$, it equals the unweighted clustering coefficient c_i for all nodes $i \in \{1, \ldots, N\}$.

Instead of counting all triangles that are associated with a certain node in the same way, the weighted clustering coefficient c_i^{w} accounts for differences in the underlying edge weights. For example, if a triangle connects nodes i, j, and k, the unweighted local clustering coefficient counts the corresponding edges while ignoring their weights. However, if all normalized weights $\tilde{w}$ that are associated with that triangle are close to 0, one may wish to weight it differently than other (more important) triangles with larger edge weights. In networks with complex weights, it is possible to account not only for positive and negative edges (which arise, *e.g.*, in correlation networks [76, 77] and in subjects such as international relations [78, 79]), but also to quantify directional and phase information (in addition to magnitudes). In Figure 3(a), we show an example of an undirected triad with weights $e^{\mathrm{i}\varphi}$. The local weighted clustering coefficient of node i is $c_i^{\mathrm{w}} = e^{\mathrm{i}\varphi}$. In the directed triad in Fig. 3(b), we use the weights $e^{\pm\mathrm{i}\varphi}$ to encode directional information. The corresponding local weighted clustering coefficient of node i is $c_i^{\mathrm{w}} = \cos(\varphi)$. This example illustrates that one can use the weighted clustering coefficient c_i^{w} to characterize the local distribution of complex edge weights. If all weights have the same magnitude and the phases that are associated with the two cycles $i \to j \to k \to i$ and $i \to k \to j \to i$ have opposite signs, then the imaginary part of c_i^{w} is 0.

IV. MATRIX POWERS AND WALKS

Given an adjacency matrix A, the entries $a_{ij}^{(k)}$ of the matrix powers A^k (with $k \in \{1, 2, \ldots\}$) correspond to the number of walks of length k that start at node i and end at node j [80]. For weight matrices W, each entry $w_{ij}^{(k)}$ of the matrix power W^k is equal to the sum of the products of all weights that are associated with length-k walks from node i to node j. If W is a stochastic matrix, the entries of W^k correspond to the probabilities of reaching certain nodes from given starting nodes.

One advantage of complex-valued weights over real-valued weights is that they can encode directional information. Consider the network in Fig. 1(b). The clockwise and counterclockwise walks have negative and positives phases, respectively. One can determine the "direction" of a walk in such a network from the accumulated phase of the product of the weights that are associated with edges that a walker traverses. For example, the walks $1 \to 2 \to 1$ and $1 \to 2 \to 3$ have total weights of $e^{\mathrm{i}0}$ and $e^{\mathrm{i}2\pi/3}$, respectively. Therefore, their phases 0 and $2\pi/3$ indicate that the first walker traverses edges of opposite phase and returns to its initial position and that the second walker moves in the counterclockwise direction. In a quantum picture, one can interpret the positive and negative phases that are associated with a walk $i \to j$ as Aharonov–Bohm phases that result from interactions between a charged particle and a magnetic vector potential $\mathbf{A}$ [29, 46]. That is,

$$\varphi_{ij} = \int_{\mathcal{C}_{ij}} \mathbf{A} \cdot \mathrm{d}\mathbf{x}\,, \tag{21}$$

where $\varphi_{ij} = -\varphi_{ji}$ and $\mathcal{C}_{ij}$ is a curve from position $\mathbf{x}_i$ to position $\mathbf{x}_j$. The amplitude r_{ij} in $w_{ij} = r_{ij}e^{\mathrm{i}\varphi_{ij}}$ is equal to a_{ij}. That is, it is equal to 1 if the charged particle can move from $\mathbf{x}_i$ to $\mathbf{x}_j$ and it is otherwise equal to 0. The resulting weight matrix is a discrete version of the magnetic Laplacian [29].

The complex edge weights $w_{ij} = e^{\mathrm{i}\pi/3} = (1 + \mathrm{i}\sqrt{3})/2$ and $w_{ji} = \bar{w}_{ij} = e^{-\mathrm{i}\pi/3} = (1 - \mathrm{i}\sqrt{3})/2$ in the directed triads in Fig. 1(b) have useful properties for applications in network analysis because both their product and sum is equal to 1 (*i.e.*, $w_{ij}w_{ji} = 1$ and $w_{ij} + w_{ji} = 1$) [44]. In the associated weight-matrix powers, a walk $i \to j \to i$ then contributes 1 just as in the corresponding adjacency-matrix powers. As an example, we again consider the network in Fig. 1(b) and calculate the square of its weight matrix W and adjacency matrix A. That is,

$$W^2 = \begin{pmatrix} 2 & e^{-\mathrm{i}2\pi/3} & e^{\mathrm{i}2\pi/3} \\ e^{\mathrm{i}2\pi/3} & 2 & e^{-\mathrm{i}2\pi/3} \\ e^{-\mathrm{i}2\pi/3} & e^{\mathrm{i}2\pi/3} & 2 \end{pmatrix}, \; A^2 = \begin{pmatrix} 2 & 1 & 1 \\ 1 & 2 & 1 \\ 1 & 1 & 2 \end{pmatrix}. \tag{22}$$

In this example, the diagonal entries of W^2 and A^2 are equivalent because of the multiplicative and additive properties of $e^{\pm\mathrm{i}\pi/3}$.

Complex weights with fractional phases such as $\varphi = \pi/3$ arise in quantum-mechanical particle statistics. Exchanging bosonic particles in a multi-particle wave function is associated with a phase $\varphi = 0$, and the exchange phase of fermions is $\varphi = \pi$. One can realize fractional phases $\varphi = \pi/(2m+1)$ (with $m \in \mathbb{N}_{>0}$) that lie between those of bosons and fermions using anyons, which are quasi-particles that arise in two-dimensional systems [55–59]. In particular, the phases $\varphi = \pi/3$ have been observed experimentally in anyon systems [58, 59]. In a network that represents anyon permutations, one obtains the total phase that is associated with a permutation by multiplying the complex weights $e^{\mathrm{i}\varphi_{ij}}$ in the $U(1)$ representation of the underlying braid group. In an anyon system with exchange phase $\varphi = \pi/3$, exchanging two particles twice is then associated with a total phase of $\varphi = 2\pi/3$, as in some off-diagonal entries of W^2 in Eq. (22).

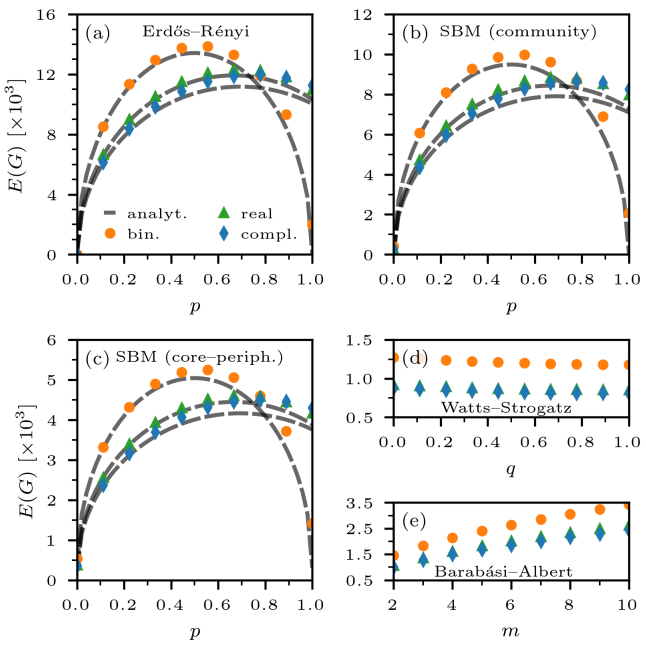

FIG. 4. **Graph energies for different networks and weight distributions.** The graph energies $E(G)$ [see Eq. (23)] for five different networks and three types of weight distributions: (a) a $G(N,p)$ ER network, (b) a stochastic block model (SBM) with two $G(N,p)$ ER blocks and inter-block connection probability 10^{-3}, (c) an SBM with one $G(N,p)$ ER block, one $G(N,p)$ ER block with $p = 10^{-3}$, and inter-block connection probability 10^{-3}, (d) a $G(N,k,q)$ Watts–Strogatz (WS) network in which each node is adjacent to $k = 2$ nearest neighbors (where q denotes the probability of rewiring each edge), and (e) a Barabási–Albert (BA) network. All of these networks have $N = 1000$ nodes. In all simulations that involve weighted networks, we use Hermitian weight matrices (*i.e.*, $W = W^\dagger$). To construct the BA network, we start with a star graph with 1 node and m leaves, and we iteratively add new nodes until there are 1000 nodes. Each new node has m edges that connect to existing nodes using linear preferential attachment. The orange disks indicate our numerical results for binary weight matrices (*i.e.*, for $W = A$). The green triangles and blue diamonds indicate our numerical results for real and complex weight distributions, respectively. The real weights are distributed uniformly in the interval $[0, 4/3)$, and the complex weights are distributed uniformly in the first quadrant of the complex plane. All reported results are means of 100 independent instantiations of the indicated random-graph model. The dashed gray curves in panels (a)–(c) are based on the analytical solutions (24), (B4), and (B5), which assume that $N \to \infty$.

V. GRAPH ENERGY

The energy of a graph is

$$E(G) = \sum_{i=1}^{N} |\lambda_i| \,, \tag{23}$$

where λ_i is the ith eigenvalue of the weight matrix W [60]. In Hückel (*i.e.*, tight-binding) molecular-orbital (HMO) theory, one typically represents conjugated hydrocarbon molecules by undirected and unweighted networks. In this situation, the energy of π-electrons in the HMO approximation is equivalent to the energy in Eq. (23) [60]. Although most applications of network analysis to mathematical chemistry have focused on undirected and unweighted molecular networks, weight matrices with real and complex entries have also been studied [33] (*e.g.*, represent cis/trans isomers of molecules [31, 32]).

In mathematical chemistry and chemical graph theory, it is common to calculate the graph energy $E(G)$ to characterize conjugated molecular structures in terms of their π-electron energy. One can obtain closed-form expressions for the graph energy of certain graphs [60]. For example, the energy of almost every[3] $G(N,p)$ ER network [60, 81] is

$$E[G(N,p)] = N^{3/2}\left(\frac{8}{3\pi}\sqrt{p(1-p)} + \mathcal{O}(1)\right) , \tag{24}$$

where p is the connection probability. There are very few energy estimates for weighted networks, so in particular there are few such estimates for networks with complex edge weights [42]. We use graph energy to characterize Erdős–Rényi, stochastic-block-model (SBM), Watts–Strogatz (WS) [82], and Barabási–Albert (BA) [83] networks with binary, real, and complex weight distributions (see Fig. 4). We study one 2-block SBM with community structure and one 2-block SBM with core–periphery structure. In our calculations, we distribute the complex weights uniformly at random in the subset of the unit circle in the first quadrant of the complex plane [*i.e.*, $\varphi_{ij} \sim \mathcal{U}(0, \pi/2)$ and $r_{ij} = \sqrt{\epsilon_{ij}}$, where $\epsilon_{ij} \sim \mathcal{U}(0,1)$] and distribute the real weights uniformly at random in the interval $[0, 4/3)$ [*i.e.*, $w_{ij} \sim \mathcal{U}(0, 4/3)$]. In our numerical experiments, the support of the uniform distribution $\mathcal{U}(a,b)$ is the half-open interval $[a,b)$. We use the interval $[0, 4/3)$ to ensure that the mean value of the real weights is equal to the mean absolute value of the complex weights. The examined weight matrices are Hermitian. In App. B, we derive analogs of Eq. (24) for ER networks with these two weight distributions.

In Figure 4, we show sample means of the graph energy $E(G)$ for ER, SBM, WS, and BA networks as a function of the underlying network model parameters. (We show the corresponding eigenvalue distributions in App. B.) For an ER network with binary edges [see Fig. 4(a)], we obtain a maximum of the graph energy in the $N \to \infty$ limit for $p = 0.5$ [see Eq. (24)], whereas the examined real and complex weight distributions are associated with a graph-energy maximum that we obtain for $p \approx 0.8$. We

[3] In this paper, we say that "almost every" graph $\hat{G}$ in a random-graph model G with N nodes has a certain property if the probability that $\hat{G}$ satisfies that property approaches 1 as $N \to \infty$.

obtain the largest difference in graph energy between the examined ER networks with binary edges and its counterparts with real and complex edge weights for $p \to 1$ (*i.e.*, in a fully connected graph). Although an unweighted ER network has a graph energy of $E[G(N, p = 1)] = 2(N - 1)$ (see App. C), the corresponding weighted networks have significantly larger values of graph energy for $p = 1$ and $N = 1000$. The graph energies of the examined SBM networks have a similar dependence on p as in the ER networks [see Fig. 4(b,c)]. For small inter-block connection probabilities, one can approximate the graph energy of an SBM network that consists of ER blocks by the sum of the corresponding ER graph energies (24).

The mean graph energy of the WS networks decreases as one increases the rewiring probability q. In the BA networks, the mean graph energy increases with m, which is the number of new edges that one adds for each new node. For the examined WS and BA networks, the mean graph energies that we obtain for binary weights are larger than those for the examined real and complex weights. Although the mean values of the selected real weights equal the means of the absolute values of the associated complex weights, the mean values of $E(G)$ for an ER network with real weights are larger than those of its counterpart with complex weights for $p \lessapprox 0.8$. For $p \gtrapprox 0.8$, the mean graph energy is larger for ER networks with complex weights than for ER networks with real or binary weights. In the WS and BA networks, the graph energies that we obtain with real weights are about 5% and 8% larger, respectively, than those with complex weights.

To summarize, graph energy is different for unweighted networks, networks with real edge weights, and networks with complex edge weights. This is the case both for the magnitude of the graph energy and for how it depends on the connectivity properties of the underlying network (as quantified by the network parameters p, q, and m). Given the described connections between graph energy and energy estimates of conjugated molecules, our results may be relevant to the modeling of molecules with weighted networks.

VI. THE PERRON–FROBENIUS THEOREM AND EIGENVECTOR CENTRALITY

According to the Perron–Frobenius theorem [61, 62], the weight matrix $W = A$ of an unweighted, strongly connected network is associated with a simple positive eigenvalue (the "Perron eigenvalue") that is strictly larger than all other eigenvalues. The Perron eigenvalue is equal to the spectral radius of W. That is, $\rho(A) \coloneqq \max_{i\in\{1,\ldots,N\}}\{|\lambda_i|\}$, where $\{\lambda_i\}_{i\in\{1,\ldots,N\}}$ is the set of eigenvalues (*i.e.*, the spectrum) of W. The corresponding Perron eigenvector (*i.e.*, the leading eigenvector) is a centrality measure [1].

The Perron–Frobenius theorem does not hold for matrices with complex weights, so we cannot find a Perron eigenvalue of W and a corresponding eigenvector to use as a centrality measure. However, generalizations of the Perron–Frobenius theorem [63, 64] provide a possible approach to define eigenvector centrality (and generalizations of it, such as PageRank) for networks with certain types of complex weight matrices. A complex weight matrix W has the "strong Perron–Frobenius property" if it (1) has a simple positive eigenvalue λ_1 that satisfies $\lambda_1 = \rho(W) > |\lambda_i|$ (with $i \in \{2, \ldots, N\}$) and (2) has a corresponding column eigenvector v_1 with positive entries. The eigenvector v_1 is called the "right Perron–Frobenius eigenvector". For further details about generalizations of the Perron–Frobenius theorem to complex matrices, see Ref. [64].

An example of a weight matrix with the strong Perron–Frobenius property is

$$W = \begin{pmatrix} 0 & ae^{\mathrm{i}\varphi_a} & 0 \\ be^{\mathrm{i}\varphi_b} & 0 & ce^{\mathrm{i}\varphi_c} \\ 0 & de^{\mathrm{i}\varphi_d} & 0 \end{pmatrix} \tag{25}$$

with $a = b = c = 1$, $d = -1/2$, $\varphi_a = 0$, $\varphi_b = \pi/6$, $\varphi_c = 3\pi/2$, and $\varphi_d = \pi$. That is,

$$W = \begin{pmatrix} 0 & 1 & 0 \\ e^{\mathrm{i}\pi/6} & 0 & -\mathrm{i} \\ 0 & 1/2 & 0 \end{pmatrix} . \tag{26}$$

The largest eigenvalue of W is $\sqrt[4]{3/4}$, and its corresponding eigenvector is $v_1 = (2, \sqrt[4]{12}, 1)^\top$. What is the meaning of the right Perron–Frobenius vector $v_1 = (2, \sqrt[4]{12}, 1)^\top$ in the context of the eigenvector centrality of a complex weight matrix? In this example, nodes 1, 2, and 3 have eigenvector centralities of 2, $\sqrt[4]{12}$, and 1, respectively. The most central nodes in the associated network are thus nodes 1 and 2, whereas node 3 (which has a single out-edge with weight 1/2) ranks third. In this example, the eigenvector centralities that we obtain using the complex weight matrix W coincide with the eigenvector centralities that we obtain from $\mathrm{Re}(W)$.

In App. D, we show that any two-node network with a complex Hermitian weight matrix cannot satisfy the strong Perron–Frobenius property.

VII. BETWEENNESS AND CLOSENESS CENTRALITIES

The geodesic betweenness centrality $c_{\mathrm{B}}(i)$ of a node i quantifies the number of shortest paths that traverse that node, and the closeness centrality $c(i)$ of a node i quantifies the mean distance between that node and other nodes [1]. Mathematically, the normalized geodesic betweenness centrality of node i in a directed network is

$$c_{\mathrm{B}}(i) = \frac{1}{(N-1)(N-2)} \sum_{\{j,k|j\neq i,k\neq i\}} \frac{\sigma_{jk}(i)}{\sigma_{jk}} , \tag{27}$$

where σ_{jk} is the total number of shortest paths between nodes j and k and $\sigma_{jk}(i)$ is the number of those shortest

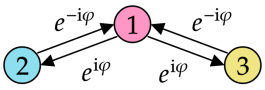

	1	2	3
betweenness	1	0	0
closeness	1	2/3	2/3

FIG. 5. **Betweenness and closeness centralities of a small network.** A network with three nodes and the weight matrix (29). The table gives the geodesic betweenness and closeness centralities of nodes 1, 2, and 3 that are associated with the unweighted analog of the depicted network.

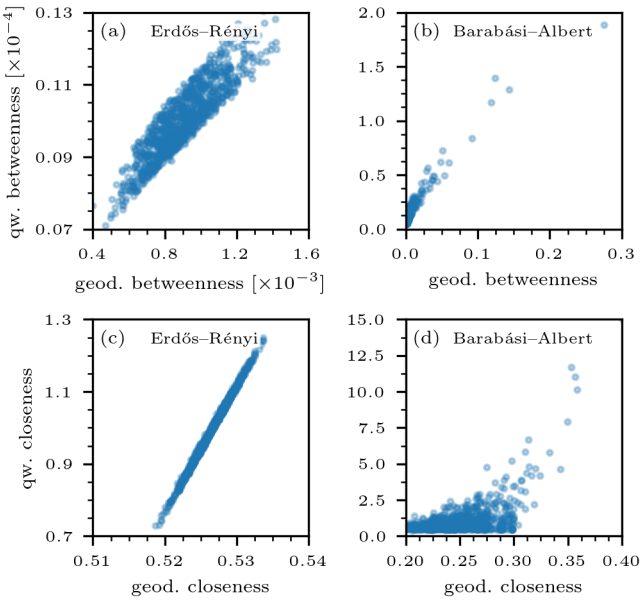

FIG. 6. **Quantum random-walk versus geodesic betweenness and closeness centralities.** We illustrate the correlations between quantum random-walk (qw) and geodesic centralities for (a,b) betweenness and (c,d) closeness. In (a,c), we show scatter plots for a $G(N,p)$ ER network with $p = 0.1$. In (b,d), we show scatter plots for a BA network that we construct from an initial star graph with 1 node and 2 leaves by iteratively adding new nodes until there are $N = 1000$ nodes. Each new node has $m = 2$ edges that connect to existing nodes using linear preferential attachment. Both networks have 1000 nodes. The Pearson correlation coefficients are (a) 0.89, (b) 0.81, (c) 1.00, and (d) 0.36. We calculate the geodesic centralities for unweighted networks. To calculate the quantum random-walk centralities, we use $H_q = -W$ [see Eq. (4)] as the evolution operator. We distribute the weights uniformly at random in the first quadrant of the complex plane, and the weight matrix satisfies $W = W^\dagger$.

paths that traverse node i. The closeness centrality of node i is

$$c(i) = \frac{N-1}{\sum_{j\neq i} d_{ij}}\,, \tag{28}$$

where d_{ij} is the geodesic (*i.e.*, shortest-path) distance between nodes i and j.

Because complex numbers are not fully ordered, one cannot use geodesic betweenness and closeness centrality measures that are based on shortest paths on networks with complex weights. Except in degenerate situations, one cannot order path lengths in networks with complex edge weights. As in the above examples for occupation and eigenvector centralities (see Secs. II and VI), one has to appropriately generalize geodesic betweenness and closeness centralities. One possibility to quantify node importance in a network with a complex weight matrix is to use quantum random-walk centrality measures [24]. In Eq. (5), we give an occupation centrality measure that is based on a quantum walk with Hamiltonian $H_q = -W$ and Hermitian W. In App. E, we describe corresponding generalizations of betweenness and closeness that are based on absorbing walks and can take complex weight matrices as inputs.

We first apply these centrality measures to a network with three nodes (see Fig. 5) and weight matrix

$$W = \begin{pmatrix} 0 & e^{i\varphi} & e^{i\varphi} \\ e^{-i\varphi} & 0 & 0 \\ e^{-i\varphi} & 0 & 0 \end{pmatrix}. \tag{29}$$

In the unweighted version of this network, the geodesic betweenness centralities of nodes 1, 2, and 3 are 1, 0, and 0, respectively. The corresponding quantum random-walk betweenness centralities that are associated with the Hamiltonian $H_q = -W$ with $\varphi = \pi/3$ are 1, 0.65, and 0.65. (We normalize the betweenness values so that the maximum is 1.) The ranking of the nodes is the same as with geodesic betweenness centrality. To calculate a quantum random-walk version of closeness centrality (see App. E), we first calculate the mean return time (*i.e.*, the inverse of the occupation probability). We calculate quantum random-walk occupation centrality π_j (with $j \in \{1,2,3\}$) by evaluating the infinite-time mean (5), where $|\psi(t)\rangle = e^{-iH_q t}\,|\psi(0)\rangle$. We set $|\psi(0)\rangle = (1,1,1)^\top/\sqrt{3}$ and find that the infinite-time mean is $\boldsymbol{\pi} = (0.5, 0.25, 0.25)^\top$. In this example, the occupation centrality of node 1 is twice as large as that of nodes 2 and 3. The corresponding quantum random-walk closeness values are 1, 0.9, and 0.9. (As with betweenness, we normalize these values so that the maximum is 1.) As with betweenness centrality, we find that quantum random-walk closeness results in the same node ranking as with geodesic closeness.

We now compare geodesic and quantum random-walk centralities for ER and BA networks with $N = 1000$ nodes and complex edge weights that we distribute uniformly at random in the subset of the unit circle in the first quadrant of the complex plane (as in our examination of graph energy). As in the prior example, the evolution operator is $H_q = -W$ [see Eq. (4)]. In Figure 6, we show scatter plots to compare the quantum random-walk and geodesic centralities. The Pearson correlation coefficients are between 0.36 and 1.00 for geodesic closeness and betweenness in the examined ER and BA networks. Our results suggest that quantum random-walk closeness and betweenness centralities are able to rank node importance

in networks with complex weights in a manner that is similar to their corresponding geodesic centralities.

VIII. CONCLUSIONS AND DISCUSSION

Networks with complex weights arise in a variety of situations. However, most studies of weighted networks have focused primarily on networks with real-valued edge weights.

In the present paper, we examined network-analysis methods that are useful to study the structure of networks with complex edge weights. To physically interpret such networks and the underlying directional information that is encoded in the phases of the complex weights, we discussed connections between complex weight matrices and salient physical systems. For example, one can interpret phases that are associated with walks in a network with complex weights as phases that result from the interaction between a charged particle that traverses edges and interacts with a vector potential. Moreover, akin to the interpretation of stochastic weight matrices as generators of linear diffusion dynamics (*i.e.*, random walks), we showed that one can interpret Hermitian weight matrices with complex entries as generators of time translation in continuous-time quantum walks. We also generalized the DeGroot model of consensus dynamics to networks with complex edge weights. Finally, we characterized the structural features of networks with complex edge weights using a variety of network measures (specifically, generalizations of node strength and a local clustering coefficient, graph energy, and common centrality measures).

Given the diverse range of applications of networks with complex weights (see Tab. I), there are many interesting directions for future work. To analytically characterize graph energy in networks with both real and complex weights, it may be helpful to study connections between graph energy and random-matrix-theory results in weighted networks [84]. The importance of the Perron–Frobenius theorem for dynamical processes and centrality measures for networks with real weights motivates the identification of physical systems that are associated with complex weight matrices that satisfy the strong Perron–Frobenius property. Studying such connections may help further guide the development of suitable centralities, spectral clustering methods [85], and other network measures to study physical systems with complex weight matrices. Additionally, given the relevance of motifs in the study of both unweighted and weighted networks, it seems worthwhile to examine motifs in networks with complex weights, such as by generalizing walk-based motifs from classical contexts [86] to quantum ones.

ACKNOWLEDGMENTS

We thank Karen Daniels and Malte Henkel for helpful comments.

DATA AND CODE AVAILABILITY

The code and data that support the findings of the present study are publicly available at `https://gitlab.com/ComputationalScience/complex-weights`.

Appendix A: Quantum synchronization

The quantum-state evolution (8) conserves the L_2 norm that is associated with $|\psi_i\rangle$. That is, $\partial_t \|\psi_i\|^2 = \langle \partial_t \psi_i | \psi_i \rangle + \langle \psi_i | \partial_t \psi_i \rangle = 0$ because

$$\begin{aligned} \langle \psi_i | \partial_t \psi_i \rangle &= \sum_{j=1}^{N} a_{ij} \left[\langle \psi_i | \psi_j \rangle - \langle \psi_j | \psi_i \rangle \right] , \\ \langle \partial_t \psi_i | \psi_i \rangle &= \sum_{j=1}^{N} a_{ij} \left[\langle \psi_j | \psi_i \rangle - \langle \psi_i | \psi_j \rangle \right] . \end{aligned} \tag{A1}$$

Appendix B: Eigenvalue distributions

In Fig. 7, we show the eigenvalue distributions of W for the networks that we studied in Sec. V. The analytical results in Fig. 7(a) (see the solid gray curves) are based on a connection between the examined weight matrices and Wigner matrices [87]. A Wigner matrix X_N is a real symmetric matrix with entries x_{ij} (with $i, j \in \{1, \ldots, N\}$) that satisfy the following properties [60]:

- the entries x_{ij} are independent random variables with $x_{ij} = x_{ji}$;
- the diagonal entries x_{ii} are distributed according to F_1, and the off-diagonal entries x_{ij} (with $i \neq j$) are distributed according to F_2 ;
- the distribution F_2 has finite variance $\mathrm{Var}(x_{ij}) \equiv \sigma_2^2$ (*i.e.*, $\sigma_2^2 < \infty$).

In the limit $N \to \infty$, the eigenvalue distribution of a normalized Wigner matrix X_N/N converges almost surely to the Wigner semicircle distribution

$$\phi(x) = \frac{1}{2\pi\sigma_2^2} \sqrt{4\sigma_2^2 - x^2}\, \mathbb{1}_{|x|<2\sigma_2} . \tag{B1}$$

For a $G(N,p)$ ER network with binary weights, $\sigma_2^2 = p(1-p)$, which yields the $\sqrt{p(1-p)}$ term in Eq. (24).

The weights w_{ij} (with $i \neq j$) of the $G(N,p)$ ER networks with real-valued weight matrices that we studied in Sec. V are

$$w_{ij} = w_{ji} = \begin{cases} x_{ij} , & \text{with prob. } p \\ 0 , & \text{with prob. } 1-p , \end{cases} \tag{B2}$$

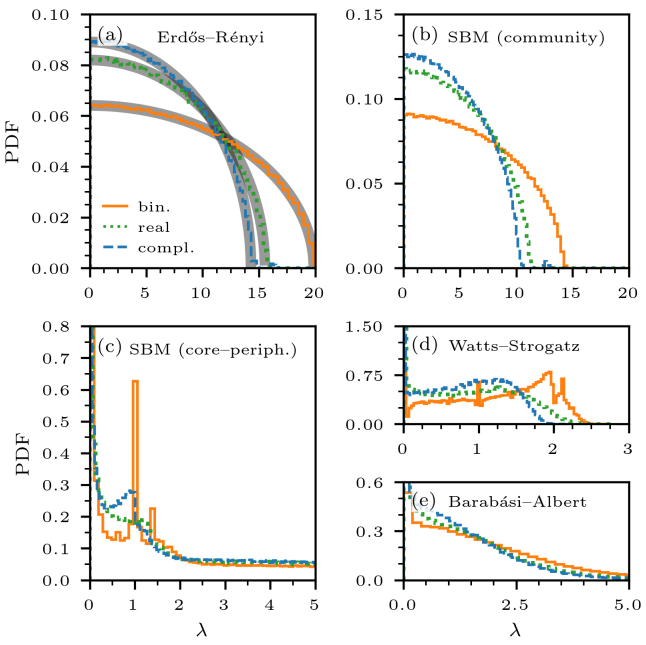

FIG. 7. **Eigenvalue distributions for different networks and weight distributions.** We show the eigenvalue distributions for five different networks and three types of weight distributions: (a) a $G(N,p)$ ER network with $p=1/9$ (where p is the connection probability), (b) an SBM with two $G(N,p)$ ER blocks with $p=1/9$ and inter-block connection probability 10^{-3}, (c) an SBM with one $G(N,p)$ ER block with $p=1/9$, one $G(N,p)$ ER block with $p=10^{-3}$, and inter-block connection probability 10^{-3}, (d) a $G(N,k,q)$ WS network in which $q=0.2$ and each node is adjacent to $k=2$ nearest neighbors (where q is the probability of rewiring each edge), and (e) a BA network. All of these networks have $N=1000$ nodes. In all simulations with weighted networks, we use Hermitian weight matrices (*i.e.*, $W=W^\dagger$). To construct the the BA network, we start with a star graph with 1 node and 2 leaves and iteratively add new nodes until there are $N=1000$ nodes. Each new node has $m=2$ edges that connect to existing nodes using linear preferential attachment. The solid orange lines indicate numerical results for binary weight matrices (*i.e.*, for $W=A$). The dotted green lines and dashed blue lines indicate numerical results for real and complex weight distributions, respectively. We distribute the real weights are distributed uniformly at random in the interval $[0,4/3)$, and we distribute the complex weights uniformly at random in the first quadrant of the complex plane. Each result is a mean of 100 independent instantiations of the indicated random-graph model The solid gray curves in panel (a) indicate the analytical solution (B1) for $\sigma_2^2=p(1-p)$, $\sigma_2^2=4(4-3p)p/27$, and $\sigma_2^2=p/2-32p^2/(9\pi^2)$ [see Eqs. (B3)–(B5)].

where $x_{ij}\sim\mathcal{U}(a,b)$ and $\mathcal{U}(a,b)$ denotes the uniform distribution on the interval $[a,b)$. The corresponding variance is

$$\begin{aligned}\sigma_2^2 &= \frac{p}{b-a}\int_a^b x^2\,\mathrm{d}x - \frac{p^2(b-a)^2}{4}\\ &= \frac{1}{12}p\left[4(a^2+ab+b^2)-3(a-b)^2p\right]\,.\end{aligned} \tag{B3}$$

For $x_{ij}\sim U(0,4/3)$ (with $i\neq j$), the energy of almost every $G(N,p)$ ER network with real-valued weights (see Sec. V) is

$$E[G(N,p)] = N^{3/2}\left(\frac{8}{3\pi}\sqrt{\frac{4(4-3p)p}{27}}+\mathcal{O}(1)\right)\,. \tag{B4}$$

For the $G(N,p)$ ER network with complex-valued weights that we studied in the main manuscript, a similar calculation yields

$$E[G(N,p)] = N^{3/2}\left(\frac{8}{3\pi}\sqrt{\frac{p}{2}-\frac{32p^2}{9\pi^2}}+\mathcal{O}(1)\right)\,, \tag{B5}$$

where we used the relations $\mathrm{Var}(Z)=\mathrm{Var}(\mathrm{Re}(Z))+\mathrm{Var}(\mathrm{Im}(Z))$ and $\mathrm{Var}(XY)=(\sigma_X^2+\mu_X^2)(\sigma_Y^2+\mu_Y^2)-\mu_X^2\mu_Y^2$, where μ_X and σ_X^2 denote the mean and variance of the random variable X. Although the semicircle law (B1) has been derived for real symmetric matrices, generalizations to complex-valued Hermitian matrices have also been studied (see, *e.g.*, Ref. [88]).

Appendix C: Erdős–Rényi (ER) graph energy with $p\to 1$

In the limit $p\to 1$, a $G(N,p)$ ER network has the expected adjacency matrix

$$A = uu^\top - \mathbb{1}\,, \tag{C1}$$

where $u\in\mathbb{R}^N$ is a vector whose entries are equal to 1. We calculate the eigenvalues of A by distinguishing two cases of the eigenvalue equation $Av=\langle u,v\rangle u - v=\lambda v$. For the $N-1$ eigenvectors that are orthogonal to u, we have $\langle u,v\rangle=0$. The corresponding eigenvalue (of multiplicity $N-1$) is -1. The remaining eigenvector $v=u$ is associated with the eigenvalue $N-1$.

In the limit $p\to 1$, the energy of almost every unweighted $G(N,p)$ ER network is

$$E[G(N,p)] = \sum_{i=1}^N |\lambda_i| = 2(N-1)\,. \tag{C2}$$

Appendix D: No Hermitian two-node Networks with complex edge weights satisfy the strong Perron–Frobenius property

Consider a general two-node network with complex edge weights and Hermitian weight matrix

$$W = \begin{pmatrix} a & be^{\mathrm{i}\varphi}\\ be^{-\mathrm{i}\varphi} & c\end{pmatrix}\,, \tag{D1}$$

where $a, b, c \in \mathbb{R}_{\geq 0}$ and $\varphi \in [0, 2\pi)$. Equation (D1) allows self-weights. The largest eigenvalue of W is

$$\frac{1}{2}\left(a + c\sqrt{(a-c)^2 + 4b^2}\right), \tag{D2}$$

and the corresponding eigenvector is

$$\left(\frac{e^{\mathrm{i}\varphi}(a - c + \sqrt{(a-c)^2 + 4b^2})}{2b}, 1\right)^{\top}. \tag{D3}$$

The imaginary part of the off-diagonal components of W is 0 for $\varphi = 0$ or $\varphi = \pi$. However, for the eigenvector (D3) to be positive, the phase φ must be either 0 or π. Therefore, the imaginary part of the off-diagonal entries of W [see Eq. (D1)] is 0. Consequently, it is not possible to have a two-node network with a Hermitian weight matrix that has off-diagonal matrix entries with non-zero imaginary part and satisfies the strong Perron–Frobenius property [64].

Appendix E: Quantum random-walk betweenness and closeness centralities

In the main manuscript, we used the infinite-time mean (5) of a CTQW [see Eq. (4)] to define the occupation centralities of the nodes of a network with a Hermitian weight matrix W. To characterize betweenness and closeness centralities of the nodes of a network with complex weights, we first define the absorbing quantum random-walk Hamiltonian

$$[(H_\ell)^{\mathrm{a}}_{\mathrm{q}}]_{ij} = \begin{cases} (H_{\mathrm{q}})_{ij}\,, & \text{if } j \neq \ell \\ 0\,, & \text{if } j = \ell \end{cases} \tag{E1}$$

with absorbing node ℓ. The basic idea that underlies the use of an absorbing Hamiltonian is that we wish to track the number of times that a quantum random walker traverses a node if its final destination is ℓ [24, 67]. Taking a mean over all absorbing nodes yields a measure of random-walk betweenness centrality. Note that $(H_\ell)^{\mathrm{a}}_{\mathrm{q}}$ is a non-Hermitian operator. To evaluate its infinite-time mean (5), we treat the upper triangular part of $(H_\ell)^{\mathrm{a}}_{\mathrm{q}}$ as equal to the conjugate transpose of the lower triangular part. To do so, we use eigenvalue-problem solvers such as `scipy.linalg.eigh` (SCIPY version 1.9.1) and `numpy.linalg.eigh` (NUMPY version 1.23), which treat non-Hermitian matrices as Hermitian matrices. We denote the corresponding Hermitian version of $(H_\ell)^{\mathrm{a}}_{\mathrm{q}}$ by $(\widetilde{H}_\ell)^{\mathrm{a}}_{\mathrm{q}}$.

The quantum random-walk betweenness centrality of node j is

$$\tau_j = \lim_{s\to 0} \frac{1}{N(N-1)} \sum_{\ell} \sum_{m,n} \frac{\langle e_m^{(\ell)}|\psi(0)\rangle \langle \psi(0)|e_n^{(\ell)}\rangle}{s + \mathrm{i}(\lambda_m^{(\ell)} - \lambda_n^{(\ell)})} \langle j|e_m^{(\ell)}\rangle \langle e_n^{(\ell)}|j\rangle\,, \tag{E2}$$

where $|\psi(0)\rangle = (1, \ldots, 1)^{\top}/\sqrt{N}$ and $e_m^{(\ell)}$ and $\lambda_m^{(\ell)}$, respectively, are the orthonormal eigenvectors and corresponding eigenvalues of the Hamiltonian $(\widetilde{H}_\ell)^{\mathrm{a}}_{\mathrm{q}}$ [24]. That is,

$$(\widetilde{H}_\ell)^{\mathrm{a}}_{\mathrm{q}} e_m^{(\ell)} = \lambda_m^{(\ell)} e_m^{(\ell)}\,, \quad \langle e_m^{(\ell)}|e_n^{(\ell)}\rangle = \delta_{mn}\,. \tag{E3}$$

We use the regularization parameter s in Eq. (E2) to prevent the denominator from equaling 0 when $\lambda_m^{(\ell)} = \lambda_n^{(\ell)}$. In all of our numerical experiments, we set $s = 10^{-1}$.

The quantum random-walk closeness centrality of node ℓ is equal to the inverse of the mean first-passage time h_ℓ of a walker that starts at any node and stops after reaching node ℓ. The mean first-passage time is

$$h_\ell = \frac{1}{N-1} \sum_{i,j} (\tau_\ell)_{ij} + \frac{1}{N} \pi_\ell^{-1}\,, \tag{E4}$$

where $(\tau_\ell)_{ij}$ denotes the expected number of times that a random walker that starts at node i with final destination ℓ traverses node j at any time. As in Eq. (E2), we do not sum over all initial nodes i; instead, we consider a uniform initial walker state $|\psi(0)\rangle = (1, \ldots, 1)^{\top}/\sqrt{N}$ and compute $\sum_j (\tau_\ell)_j$ in terms of Eq. (E2) by replacing the sum over ℓ with a sum over j. The quantity π_ℓ^{-1} is the inverse of the occupation probability (5) (*i.e.*, the mean return time).

For more information on classical and quantum random-walk centrality measures and their generalizations to multilayer networks, see Refs. [24, 67].

[1] M. E. J. Newman, *Networks*, 2nd ed. (Oxford University Press, Oxford, UK, 2018).

[2] M. A. Porter and J. P. Gleeson, *Dynamical Systems on Networks: A Tutorial*, Frontiers in Applied Dynamical Systems: Reviews and Tutorials, Vol. 4 (Springer International Publishing, Cham, Switzerland, 2016).

[3] M. Salathé, M. Kazandjieva, J. W. Lee, P. Levis, M. W. Feldman, and J. H. Jones, A high-resolution human contact network for infectious disease transmission, Proc. Natl. Acad. Sci. U.S.A. **107**, 22020 (2010).

[4] A. Barrat, M. Barthelemy, R. Pastor-Satorras, and A. Vespignani, The architecture of complex weighted networks, Proc. Natl. Acad. Sci. U.S.A. **101**, 3747 (2004).

[5] A. A. S. T. Ribeiro and V. Ortiz, Determination of signaling pathways in proteins through network theory: importance of the topology, J. Chem. Theory Comput. **10**, 1762 (2014).

[6] M. E. J. Newman, Analysis of weighted networks, Phys. Rev. E **70**, 056131 (2004).

[7] J.-P. Onnela, J. Saramäki, J. Kertész, and K. Kaski, Intensity and coherence of motifs in weighted complex networks, Phys. Rev. E **71**, 065103 (2005).

[8] J. Saramäki, M. Kivelä, J.-P. Onnela, K. Kaski, and J. Kertesz, Generalizations of the clustering coefficient to weighted complex networks, Phys. Rev. E **75**, 027105 (2007).

[9] S. Horvath, *Weighted Network Analysis: Applications in Genomics and Systems Biology* (Springer-Verlag, Heidelberg, Germany, 2011).

[10] G. J. Li and M. A. Porter, A bounded-confidence model of opinion dynamics with heterogeneous node-activity levels, arXiv:2206.09490 (2022).

[11] W. Heisenberg, Über quantentheoretische Umdeutung kinematischer und mechanischer beziehungen., Z. Phys. **33**, 879 (1925).

[12] E. Schrödinger, Quantisierung als Eigenwertproblem, Ann. Phys. **386**, 109 (1926).

[13] P. A. M. Dirac, *The Principles of Quantum Mechanics* (Oxford University Press, Oxford, UK, 1930).

[14] M. McKague, M. Mosca, and N. Gisin, Simulating quantum systems using real Hilbert spaces, Phys. Rev. Lett. **102**, 020505 (2009).

[15] M.-O. Renou, D. Trillo, M. Weilenmann, T. P. Le, A. Tavakoli, N. Gisin, A. Acín, and M. Navascués, Quantum theory based on real numbers can be experimentally falsified, Nature **600**, 625 (2021).

[16] M.-C. Chen, C. Wang, F.-M. Liu, J.-W. Wang, C. Ying, Z.-X. Shang, Y. Wu, M. Gong, H. Deng, F.-T. Liang, *et al.*, Ruling out real-valued standard formalism of quantum theory, Phys. Rev. Lett. **128**, 040403 (2022).

[17] Z.-D. Li, Y.-L. Mao, M. Weilenmann, A. Tavakoli, H. Chen, L. Feng, S.-J. Yang, M.-O. Renou, D. Trillo, T. P. Le, *et al.*, Testing real quantum theory in an optical quantum network, Phys. Rev. Lett. **128**, 040402 (2022).

[18] M. Faccin, P. Migdał, T. H. Johnson, V. Bergholm, and J. D. Biamonte, Community detection in quantum complex networks, Phys. Rev. X **4**, 041012 (2014).

[19] J. Biamonte, M. Faccin, and M. De Domenico, Complex networks from classical to quantum, Commun. Phys. **2**, 53 (2019).

[20] A. Muranova and W. Woess, Networks with complex weights: Green function and power series, Mathematics **10**, 820 (2022).

[21] S. H. Strub and L. Böttcher, Modeling deformed transmission lines for continuous strain sensing applications, Meas. Sci. Technol. **31**, 035109 (2019).

[22] A. M. Childs and J. Goldstone, Spatial search by quantum walk, Phys. Rev. A **70**, 022314 (2004).

[23] R. Portugal, *Quantum Walks and Search Algorithms* (Springer-Verlag, Heidelberg, Germany, 2013).

[24] L. Böttcher and M. A. Porter, Classical and quantum random-walk centrality measures in multilayer networks, SIAM J. Appl. Math. **81**, 2704 (2021).

[25] S. Kubota, E. Segawa, and T. Taniguchi, Quantum walks defined by digraphs and generalized Hermitian adjacency matrices, Quantum Inf. Process. **20**, 1 (2021).

[26] K. Kadian, S. Garhwal, and A. Kumar, Quantum walk and its application domains: A systematic review, Comput. Sci. Rev. **41**, 100419 (2021).

[27] C.-H. Wu and G. Mahler, Quantum network theory of transport with application to the generalized Aharonov–Bohm effect in metals and semiconductors, Phys. Rev. B **43**, 5012 (1991).

[28] Y. Liu, Z. Hou, P. M. Hui, and W. Sritrakool, Electronic transport properties of Sierpinski lattices, Phys. Rev. B **60**, 13444 (1999).

[29] E. H. Lieb and M. Loss, Fluxes, Laplacians, and Kasteleyn's Theorem, Duke Math. J. **71**, 337 (1993).

[30] P. Vasilopoulos, O. Kálmán, F. M. Peeters, and M. G. Benedict, Aharonov–Bohm oscillations in a mesoscopic ring with asymmetric arm-dependent injection, Phys. Rev. B **75**, 035304 (2007).

[31] G. Lekishvili, On the characterization of molecular stereostructure: 1. Cis–trans isomerism, J. Chem. Inf. Comput. Sci. **37**, 924 (1997).

[32] A. Golbraikh, D. Bonchev, and A. Tropsha, Novel ZE-isomerism descriptors derived from molecular topology and their application to QSAR analysis, J. Chem. Inf. Comput. Sci. **42**, 769 (2002).

[33] E. Estrada, J. A. Rodríguez-Velázquez, and M. Randić, Atomic branching in molecules, Int. J. Quantum Chem. **106**, 823 (2006).

[34] C. R. Paul, *Analysis of multiconductor transmission lines* (John Wiley & Sons, Hoboken, NJ, USA, 2007).

[35] R. S. Lakes, *Viscoelastic Materials* (Cambridge University Press, Cambridge, UK, 2009).

[36] B. Hoser and A. Geyer-Schulz, Eigenspectral analysis of Hermitian adjacency matrices for the analysis of group substructures, J. Math. Soc. **29**, 265 (2005).

[37] H. Zhang, M. Gu, X. D. Jiang, J. Thompson, H. Cai, S. Paesani, R. Santagati, A. Laing, Y. Zhang, M. H. Yung, Y. Z. Shi, F. K. Muhammad, G. Q. Lo, X. S. Luo, B. Dong, D. L. Kwong, L. C. Kwek, and A. Q. Liu, An optical neural chip for implementing complex-valued neural network, Nat. Commun. **12**, 457 (2021).

[38] X. Zhang, Y. He, N. Brugnone, M. Perlmutter, and M. J. Hirn, MagNet: A Neural Network for Directed Graphs, in *Advances in Neural Information Processing Systems 34: Annual Conference on Neural Information Processing Systems 2021, NeurIPS 2021, December 6–14, 2021, virtual*, edited by M. Ranzato, A. Beygelzimer, Y. N. Dauphin, P. Liang, and J. W. Vaughan (2021) pp. 27003–27015.

[39] Y. He, M. Perlmutter, G. Reinert, and M. Cucuringu, MSGNN: A Spectral Graph Neural Network Based on a Novel Magnetic Signed Laplacian, arXiv preprint arXiv:2209.00546 (2022).

[40] S. Furutani, T. Shibahara, M. Akiyama, K. Hato, and M. Aida, Graph Signal Processing for Directed Graphs Based on the Hermitian Laplacian, in *Machine Learning and Knowledge Discovery in Databases - European Conference, ECML PKDD 2019, Würzburg, Germany, September 16-20, 2019, Proceedings, Part I*, Lecture Notes in Computer Science, Vol. 11906, edited by U. Brefeld, É. Fromont, A. Hotho, A. J. Knobbe, M. H. Maathuis, and C. Robardet (Springer, Heidelberg, DE, 2019) pp. 447–463.

[41] M. Cucuringu, H. Li, H. Sun, and L. Zanetti, Hermitian matrices for clustering directed graphs: insights and applications, in *The 23rd International Conference on Artificial Intelligence and Statistics, AISTATS 2020, 26-28 August 2020, Online [Palermo, Sicily, Italy]*, Proceedings of Machine Learning Research, Vol. 108, edited by S. Chiappa and R. Calandra (PMLR, 2020).

[42] J. Liu and X. Li, Hermitian-adjacency matrices and Hermitian energies of mixed graphs, Linear Algebra Appl. **466**, 182 (2015).

[43] K. Guo and B. Mohar, Hermitian adjacency matrix of digraphs and mixed graphs, J. Graph Theory **85**, 217 (2017).

[44] B. Mohar, A new kind of Hermitian matrices for digraphs, Linear Algebra Appl. **584**, 343 (2020).

[45] S. Kubota, H. Sekido, and H. Yata, Periodicity of quantum walks defined by mixed paths and mixed cycles, Linear Algebra Appl. **630**, 15 (2021).

[46] J. E. Avron, A. Raveh, and B. Zur, Adiabatic quantum transport in multiply connected systems, Rev. Mod. Phys. **60**, 873 (1988).

[47] U. Smilansky, Discrete Graphs – A Paradigm Model for Quantum Chaos, in *Chaos: Poincaré Seminar 2010*, edited by B. Duplantier, S. Nonnenmacher, and V. Rivasseau (Springer-Verlag, Heidelberg, Germany, 2013) pp. 97–124.

[48] T. Peron, B. M. F. de Resende, F. A. Rodrigues, L. d. F. Costa, and J. A. Méndez-Bermúdez, Spacing ratio characterization of the spectra of directed random networks, Phys. Rev. E **102**, 062305 (2020).

[49] N. Masuda, M. A. Porter, and R. Lambiotte, Random walks and diffusion on networks, Phys. Rep. **716**, 1 (2017).

[50] M. A. Lohe, Non-Abelian Kuramoto models and synchronization, J. Phys. A **42**, 395101 (2009).

[51] M. A. Lohe, Quantum synchronization over quantum networks, J. Phys. A **43**, 465301 (2010).

[52] S.-H. Choi and S.-Y. Ha, Quantum synchronization of the Schrödinger–Lohe model, J. Phys. A **47**, 355104 (2014).

[53] S.-H. Choi, J. Cho, and S.-Y. Ha, Practical quantum synchronization for the Schrödinger–Lohe system, J. Phys. A **49**, 205203 (2016).

[54] P. Antonelli and D. N. Reynolds, Schrödinger-Lohe type models of quantum synchronization with nonidentical oscillators (2022), arXiv:2210.17498.

[55] J. M. Leinaas and J. Myrheim, On the theory of identical particles, Nuovo Cim. Soc. Ital. Fis. B **37**, 1 (1977).

[56] F. Wilczek, Magnetic flux, angular momentum, and statistics, Phys. Rev. Lett. **48**, 1144 (1982).

[57] F. Wilczek, Quantum mechanics of fractional-spin particles, Phys. Rev. Lett. **49**, 957 (1982).

[58] H. Bartolomei, M. Kumar, R. Bisognin, A. Marguerite, J.-M. Berroir, E. Bocquillon, B. Pla??ais, A. Cavanna, Q. Dong, U. Gennser, Y. Jin, and G. F??ve, Fractional statistics in anyon collisions, Science **368**, 173 (2020).

[59] J. Nakamura, S. Liang, G. C. Gardner, and M. J. Manfra, Direct observation of anyonic braiding statistics, Nat. Phys. **16**, 931 (2020).

[60] X. Li, Y. Shi, and I. Gutman, *Graph Energy* (Springer-Verlag, Heidelberg, Germany, 2012).

[61] O. Perron, Zur Theorie der Matrices, Math. Ann. **64**, 248 (1907).

[62] G. Frobenius, *??ber Matrizen aus nichtnegativen Elementen* (S.-B. Preuss Acad. Wiss., Berlin, Germany, 1912).

[63] S. M. Rump, Perron–Frobenius theory for complex matrices, Linear Algebra Appl. **363**, 251 (2003).

[64] D. Noutsos and R. S. Varga, On the Perron–Frobenius theory for complex matrices, Linear Algebra Appl. **437**, 1071 (2012).

[65] L. Böttcher and H. J. Herrmann, *Computational Statistical Physics* (Cambridge University Press, Cambridge, UK, 2021).

[66] T. H. Cormen, C. E. Leiserson, R. L. Rivest, and C. Stein, *Introduction to Algorithms* (MIT Press, Boston, MA, USA, 2022).

[67] A. Solé-Ribalta, M. De Domenico, S. Gómez, and A. Arenas, Random walk centrality in interconnected multilayer networks, Physica D **323**, 73 (2016).

[68] M. Faccin, T. Johnson, J. Biamonte, S. Kais, and P. Migdał, Degree distribution in quantum walks on complex networks, Phys. Rev. X **3**, 041007 (2013).

[69] R. Olfati-Saber, J. A. Fax, and R. M. Murray, Consensus and cooperation in networked multi-agent systems, Proc. IEEE **95**, 215 (2007).

[70] A. M. Childs, On the relationship between continuous-and discrete-time quantum walk, Commun. Math. Phys. **294**, 581 (2010).

[71] M. Lipton, R. Mirollo, and S. H. Strogatz, The Kuramoto model on a sphere: Explaining its low-dimensional dynamics with group theory and hyperbolic geometry, Chaos **31**, 093113 (2021).

[72] Y. Kuramoto, Self-entrainment of a population of coupled non-linear oscillators, in *International Symposium on Mathematical Problems in Theoretical Physics* (Springer-Verlag, Heidelberg, Germany, 1975) pp. 420–422.

[73] H. Sakaguchi and Y. Kuramoto, A soluble active rotater model showing phase transitions via mutual entertainment, Prog. Theor. Phys. **76**, 576 (1986).

[74] L. Q. English, Z. Zeng, and D. Mertens, Experimental study of synchronization of coupled electrical self-oscillators and comparison to the Sakaguchi-Kuramoto model, Phys. Rev. E **92**, 052912 (2015).

[75] E. Cozzo, M. Kivelä, M. De Domenico, A. Solé-Ribalta, A. Arenas, S. Gómez, M. A. Porter, and Y. Moreno, Structure of triadic relations in multiplex networks, New J. Phys. **17**, 073029 (2015).

[76] G. Costantini and M. Perugini, Generalization of clustering coefficients to signed correlation networks, PLOS One **9**, e88669 (2014).

[77] N. Masuda, M. Sakaki, T. Ezaki, and T. Watanabe, Clustering coefficients for correlation networks, Front. Neuroinformatics **12**, 7 (2018).

[78] D. Cartwright and F. Harary, Structural balance: a generalization of Heider's theory, Psychol. Rev. **63**, 277 (1956).

[79] S. A. Marvel, J. Kleinberg, R. D. Kleinberg, and S. H. Strogatz, Continuous-time model of structural balance, Proc. Natl. Acad. Sci. U.S.A. **108**, 1771 (2011).

[80] E. Estrada, *The Structure of Complex Networks: Theory and Applications* (Oxford University Press, Oxford, UK, 2012).

[81] P. Erdős and A. Rényi, On Random Graphs I, Publ. Math. Debr. **6**, 290 (1959).

[82] D. J. Watts and S. H. Strogatz, Collective dynamics of 'small-world' networks, Nature **393**, 440 (1998).

[83] A.-L. Barabási and R. Albert, Emergence of scaling in random networks, Science **286**, 509 (1999).

[84] J. W. Baron, Eigenvalue spectra and stability of directed complex networks, Phys. Rev. E (in press) (2022), arXiv:2206.13436.

[85] T. Michoel and B. Nachtergaele, Alignment and integration of complex networks by hypergraph-based spectral clustering, Phys. Rev. E **86**, 056111 (2012).

[86] A. C. Schwarze and M. A. Porter, Motifs for processes on networks, SIAM J. App. Dyn. Sys. **20**, 2516 (2021).

[87] E. P. Wigner, On the distribution of the roots of certain symmetric matrices, Ann. Math. **67**, 325 (1958).

[88] Z. D. Bai and J. Yao, On the convergence of the spectral empirical process of Wigner matrices, Bernoulli **11**, 1059 (2005).